View metadata, citation and similar papers at core.ac.uk
brought to you by CORE
provided by Archivio istituzionale della ricerca - Politecnico di Milano

ACCURACY IN THE IDENTIFICATION OF A GENERATOR THERMAL BOW

P. PENNACCHI
Dipartimento di Meccanica,
Politecnico di Milano,
Via La Masa, 34, I-20158, Milano, Italy.
paolo.pennacchi@polimi.it

A. VANIA
Dipartimento di Meccanica,
Politecnico di Milano,
Via La Masa, 34, I-20158, Milano, Italy.
andrea.vania@polimi.it

GENERATOR THERMAL BOW IDENTIFICATION

Pages: 23
Tables: 3
Figures: 20

Please send proofs to:
DR. P. PENNACCHI
Dipartimento di Meccanica,
Politecnico di Milano,
Via La Masa, 34, I-20158, Milano, Italy.

SUMMARY

Model based diagnostic techniques can be used to identify the faults that affect rotating machines. In general, the most important faults and malfunctions can be modelled by means of a suitable set of equivalent excitations that are applied to the nodes of a finite element model of the machine rotor train. Weighted least squares error methods can be used to identify the set of forces and moments that minimise the error between experimental transient vibrations and the rotor system response obtained with the simulating model.

However, the accuracy of the fault identification can be significantly influenced by the adequacy of the fault model as well as by the accuracy of the rotating machine model.

This paper shows some methods, based on basic statistics, which enable the accuracy of the fault identification to be evaluated. The capabilities of the proposed methods have been proved by the results of the identification of the shaft thermal bow of a power unit generator that exhibited abnormal vibrations during machine coastdowns. The accuracy with which the location and the severity of the fault have been estimated is analysed.

In addition to this, the results obtained by the identification of the actual faults have been compared with those provided by the identification of false faults that cause similar symptoms.

1. INTRODUCTION

The early detection of malfunctions in rotating machines can be enabled by the continuous condition monitoring of machine vibrations and process parameters. However, in order to improve the effectiveness of predictive maintenance actions, the alarm state detection provided by monitoring systems should be integrated with a fast identification of the severity and location of the impending fault.

Some different techniques can be used to identify faults in rotating machines. A first preliminary screening of the types of malfunctions that can have generated an alarm can be obtained with a fault symptom analysis. Usually, this method is based on the analysis of the harmonic pattern of the machine vibrations as well as on the analysis of the vibration trend. However, more significant information can be provided by model-based diagnostic techniques by which the dynamic behaviour of the fully assembled machine, composed of rotors, bearings and foundation structure, can be simulated. Usually, the machine rotor train is modelled with beam Finite Elements (FE), while the dynamic stiffness of the bearings is modelled with coefficients that depend on the rotating speed. In addition, the supporting structure can be modelled with a modal representation or with mechanical impedance matrices, as well.

In the end, the dynamic effects of machine faults can be simulated with suitable sets of forces and moments that are applied to nodes of the FE model of the machine rotor train. Therefore, the fault identification can be obtained by evaluating the set of excitations that minimises the error between the machine experimental vibrations and the respective numerical response provided by the simulating model. Usually, this error is called residue. In order to enable easier comparisons of the results obtained with the identification of different types of fault, normalised estimates of the residues are carried out. Weighted least square methods can be used to identify the equivalent forces and moments by which the fault has been modelled. Some fault identification methods are applied in time domain [1, 2], however, the approach

described in the paper, as well as most of the fault identification techniques has been developed in frequency domain [3, 4, 5].

The accuracy of the results provided by the proposed identification method can be affected by some factors that must be considered and controlled. For instance, a preliminary tuning of the machine model is required. In addition, the transient vibrations of the system which can be ascribed only to the impending fault that must be identified have to be estimated on the basis of experimental data collected both in normal conditions and after the fault occurrence.

Sometimes, the machine vibrations that are considered for the fault identification have been measured during rotating speed transients occurred with different thermal states. In addition, the effects of the non-linear behaviour of the system could be not negligible. Owing to this, the difference between the residues associated with the actual fault and some wrong fault can be rather small. Anyhow, some measures of the accuracy of the identified faults can be obtained with methods developed in the past by the authors [6]. Sometimes, these information showed to be very helpful to recognise the actual fault using inaccurate results as well as to detect modelling errors.

This paper shows the results provided by the analysis of the dynamic behaviour of the generator of a power unit that was affected by abnormal transient vibrations whose most probable cause was a shaft thermal bow. The results of a preliminary validation of the model used to simulate the dynamic behaviour of the generator are shown in the paper along with significant experimental data collected during runups and coastdowns.

Both extended and local bows have been modelled to simulate the experimental vibrations. In addition, also a local unbalance of the shaft has been considered as machine fault. The location as well as the magnitude and phase of the equivalent excitations associated with each type of fault have been estimated with the model-based identification method.

In the paper, the results provided by this investigation are shown and discussed. The residues associated with each identified fault are compared each other in order to determine the most

probable fault. In addition, the accuracy of the identified fault has been evaluated by means of a residue analysis.

The type of the equivalent excitations that have been identified, as well as their location along the rotor, has confirmed the assumption of the presence of a shaft thermal bow whose magnitude changed significantly during the machine coastdowns. In fact, planned shutdowns of the power unit showed a rotating speed dwell that caused a cooling of the shaft and copper bars placed in the hollow part of the generator rotor. Owing to this, the shaft bow and the synchronous vibration vectors changed. Therefore, the results obtained with the model-based diagnostic technique proved to be very likely.

In the end, in order to carry out an additional validation of the identification results, the identified excitations have been used to simulate the transient vibrations measured during a further machine transient, different from that one used for the fault identification. Also this study provided satisfactory results. This investigation has confirmed that the diagnostic method proposed for the identification of faults in rotating machines is able to provide successful results.

2. FAULT IDENTIFICATION STRATEGY

The model-based technique used in this investigation to identify machine faults is fully described in detail in [3]. This method enables simultaneous faults to be identified. An outline of this identification technique is shown below for the case of single faults only.

As said above, the dynamic effects of machine faults can be simulated with suitable sets of forces and moments that are applied to nodes of the FE model of the machine rotor train. By assuming that the system is linear and time invariant, the following equation can be written for each harmonic component, of order *n*, of the machine excitations:

$$\left[-(n\Omega)^2\mathbf{M} + i\,n\Omega\,\mathbf{D} + \mathbf{K}\right]\mathbf{X}_n = \mathbf{F}_n(\Omega) \tag{1}$$

where Ω is the machine rotating speed, **K**, **M** and **D** are the stiffness, mass and damping matrices of the fully assembled system, while the terms of the force vector $\mathbf{F}_n$ are the equivalent excitations used to model the fault that must be identified. The terms of vector $\mathbf{F}_n$ depends on the excitation frequency Ω. The quantity in the square brackets of eq. (1) is the mechanical impedance matrix of the system. The harmonic content of the excitations, as well as the number of non-null terms of vector $\mathbf{F}_n$, depends on the type of fault. A large review about fault modelling by means of equivalent force systems is illustrated in [4, 5] along with some model validations. Although eq. (1) can be written for every rotating speed of a transient, only the experimental vibration data collected for a limited number of suitable rotating speeds are analysed in order to avoid an overabundance of nearly identical observations that could cause numerical problems or identification errors and that could cause the solution of the problem to become time consuming. Some criteria used to select the rotating speeds at which significant transient vibrations can be considered are described in [5]. Eq. (1) can be solved to obtain the machine vibrations, by defining the transfer matrix $\mathbf{H}_n$ as the inverse of the mechanical impedance matrix:

$$\mathbf{X}_n = \left[-(n\Omega)^2 \mathbf{M} + i\, n\Omega\, \mathbf{D} + \mathbf{K} \right]^{-1} \mathbf{F}_n(\Omega) = \mathbf{H}_n \cdot \mathbf{F}_n(\Omega) \tag{2}$$

Usually, the absolute vibrations of the shafts are measured at a limited number of cross-sections that, often, coincide with the machine supports. Therefore, a vector $\mathbf{X}_m$, whose terms are the shaft displacements associated with the degrees of freedom (d.o.f.) along which the machine vibrations are measured, must be defined. A unique set of eqs. (2) can be written considering different rotating speed values. Then, the rows in eq. (2) are rearranged, by partitioning the transfer matrix $\mathbf{H}_n$, in order to split the vector $\mathbf{X}_m$, from the vector $\mathbf{X}_r$ whose terms are the displacements evaluated at the remaining d.o.f. of the rotor system model. Therefore, eq. (2) can be rewritten in the following form, in which any dependence on both Ω and harmonic order *n* has been omitted for the sake of brevity:

$$\begin{cases} \mathbf{X}_m = \mathbf{H}_m \cdot \mathbf{F} \\ \mathbf{X}_r = \mathbf{H}_r \cdot \mathbf{F} \end{cases} \tag{3}$$

Considering only the first set of eqs. (3) and the vector $\mathbf{X}_{ex}$, whose terms are the experimental transient vibrations that correspond to the terms of the vector $\mathbf{X}_m$, it is possible to determine the error, $\boldsymbol{\delta}$, between simulated vibrations and experimental data:

$$\boldsymbol{\delta} = \mathbf{X}_m - \mathbf{X}_{ex} = \mathbf{H}_m \cdot \mathbf{F} - \mathbf{X}_{ex} \tag{4}$$

Then, the equivalent excitations $\mathbf{F}_n$ can be estimated with weighted least squares error methods. In order to allow easier comparisons between the errors obtained with the identification of different faults, a relative error, ε_1, can be evaluated using the following expression:

$$\varepsilon_1 = \left(\frac{\left[\mathbf{X}_m - \mathbf{X}_{ex}\right]^{*\mathrm{T}} \left[\mathbf{X}_m - \mathbf{X}_{ex}\right]}{\mathbf{X}_{ex}^{*\mathrm{T}} \mathbf{X}_{ex}} \right)^{1/2} \tag{5}$$

Usually, the scalar error ε_1 is called residue. The location of the excitations $\mathbf{F}_n$ that model single or multiple faults must be changed along the rotors in order to identify the actual location of the fault. Therefore, many estimates of the residue ε_1 are provided by a fault identification process.

2.1 Fault identification accuracy

In addition, more than one type of fault could be modelled. Therefore, the most probable fault is that one with which the minimum residue is associated. This strategy allows the type, the severity and the location of the fault to be identified. However, in order to validate the results of this diagnostic approach, the accuracy of the fault identification should be evaluated. In fact, false faults could be identified if mis-tuned machine models, noised vibration signals or inaccurate monitoring data are used. Some methods have been developed by the authors to evaluate the accuracy of fault identifications carried out with model-based techniques [6].

These methods will be employed in the paper, but, for the sake of brevity, only an outline is shown hereafter. The measure of the identification accuracy is provided by suitable indexes. Depending on the fact that the residuals are computed considering the errors evaluated at different d.o.f.s and at different machine rotating speeds or selecting the vibration data evaluated at each single rotating speed or at each single d.o.f., the indexes can be classified as *global* or *partial* indexes.

After having identified the fault, that is the excitation vector $\mathbf{F}_n$, a further estimate of the residue, denoted ε_2, can be evaluated. This residue is computed, by applying the eq. (5), considering the experimental vibrations associated with all the available rotating speed data collected during the machine transient. Conversely, the residue ε_1 is evaluated using only a limited sub-set of monitoring data. Both residues ε_1 and ε_2 are global indexes. A significant difference between the residues ε_1 and ε_2 indicates a lack of accuracy.

Furthermore, the eq. (5) can be used considering simulated and experimental vibrations associated with only one rotating speed at time. Also in this case, the vector $\mathbf{X}_m$ is obtained considering the force vector $\mathbf{F}_n$, previously identified. In this way, it is possible to evaluate a set of residues, denoted ε_ω, which allows the relationships between the identification error and the rotating speed to be analysed. In the end, with a similar procedure, the eq. (5) can be used considering simulated and experimental vibrations associated with only one measurement point (d.o.f.) at time. This approach enables one to evaluate a set of residues, denoted ε_{dof}, which allows the dependence of the identification error on each degree of freedom to be analysed. The mean value, $\mu_{\varepsilon\omega}$ and $\mu_{\varepsilon dof}$, and the standard deviation, $\sigma_{\varepsilon\omega}$ and $\sigma_{\varepsilon dof}$, of the residues ε_ω and ε_{dof} can be used as measures of accuracy of the fault identification. These residues and the corresponding statistic parameters are partial indexes.

In the end, interesting results can be obtained with a correlation analysis between simulated and experimental vibration data. The real and imaginary parts of all the theoretical and the experimental vibrations can be located into the two real-valued vectors $\mathbf{X}_1$ and $\mathbf{X}_2$,

respectively. Then, the Modal Scale Factor (MSF) and the index denoted MAC (Modal Assurance Criterion), [7], can be evaluated as follows:

$$\mathrm{MSF} = \frac{\mathbf{X}_1^{\mathrm{T}} \mathbf{X}_2}{\mathbf{X}_2^{\mathrm{T}} \mathbf{X}_2} \tag{6}$$

$$\mathrm{MAC} = \frac{\left| \mathbf{X}_2^{\mathrm{T}} \mathbf{X}_1 \right|^2}{\left(\mathbf{X}_2^{\mathrm{T}} \mathbf{X}_2 \right) \left(\mathbf{X}_1^{\mathrm{T}} \mathbf{X}_1 \right)} \tag{7}$$

In general, the two indexes MSF and MAC are used in modal analysis and model updating; however, they can be applied also to many other problems. For an ideal identification of a machine fault $\mathbf{X}_1$ coincides with $\mathbf{X}_2$, so that the value of the indexes MSF and MAC is 1. Anyhow, as the identification procedure is based on a least squares method, in this application the MSF value is always very near to 1. On the contrary, the MAC index gives a measure of the dispersion of the data from the straight line whose angular coefficient is the MSF value. In addition, a linear regression analysis of the data contained in the vectors $\mathbf{X}_1$ and $\mathbf{X}_2$ can be carried out. The difference between the angular coefficient of the regression line and the ideal unity value is a further measure of accuracy of the fault identification. In the end, an additional information is represented by the value of the standard deviation of the errors obtained with the linear regression analysis.

3. CASE HISTORY

The model-based identification technique above described has been used to analyse the experimental vibrations of a 50 MW power unit. The machine rotor train was composed of an industrial gas turbine, a generator and a steam turbine (Figure 1). The two turbines were mounted at the opposite ends of the generator. A first gearbox was located between the steam turbine and the generator while a further gearbox was mounted between the gas turbine and the generator.

In order to reduce the effects on the machine dynamic behaviour due to misalignments and torque changes, the wheels of the two gearboxes were mounted on quill-shafts. In addition, two short flexible shafts were connected to the shafts of the gearbox located between the steam turbine and the generator. The gas turbine and the generator were permanently coupled, while the steam turbine could be connected with the power unit by means of a clutch. The operating speeds of gas turbine, generator and steam turbine were 3612 rpm, 3000 rpm and 6805 rpm, respectively.

The journal bearings of the steam turbine and the generator, as well as some of the bearings of the gear shafts, were equipped with XY radial proximity probes, mounted 45°Right (45°R) and 45°Left (45°L), respectively (see Figure 1). The machine vibrations were continuously measured and analysed by a condition monitoring system.

In order to simulate the dynamic behaviour of the power unit a mathematical model of the fully assembled machine has been developed. However, in this investigation, only the vibrations of the generator have been analysed. Owing to the presence of quill-shafts and flexible connecting shafts, the effects of the two turbines on the dynamic behaviour of the generator have been assumed unimportant. Therefore, the investigations described in this paper have been carried out by considering a model of the generator only.

Figure 2 shows the Finite Element (FE) model of the generator rotor. This shaft was mounted on three journal bearings. Supports #1 and #2 (Fig. 2) were located at the opposite ends of the main body of the generator while bearing #3 was mounted beyond the exciter, on the shaft end towards the connection with the steam turbine. Figure 2 shows that the part of the shaft between bearings #2 and #3 was rather long and slender in comparison with the main body of the generator. As usual, this part of the rotor was hollow. It extended from node 32 to the ending node 74 of the FE model of the rotor (see Fig. 2). Copper bars, through which rotor current flows, were placed in the shaft hollow.

The dynamic stiffness of the three journal bearings of the generator were evaluated at each rotating speed of interest, in the range from 400 rpm to 4500 rpm. Unfortunately, the modal parameters of foundation structure and pedestals were unavailable. Therefore, the dynamic properties of the foundation were modelled by means of lumped equivalent parameters. In order to validate the model of the generator, the first two critical speeds of the shaft have been considered. The experimental values of these resonances were in good accordance with the corresponding values provided by the simulating models.

Owing to this validation, the generator model showed to be satisfactorily tuned. Therefore, it was possible to suppose that it would have been adequate to identify machine faults by means of the model-based technique above described.

3.2 Experimental transient vibrations

The dynamic behaviour of the machine in transient mode was documented by numerous vibration data collected during many runups and coastdowns. In general, during the runups occurred when the machine is cold, the 1X vibrations of the generator were significantly different from those measured during planned machine shutdowns, which occur with the machine in a warm steady thermal state. Anyhow, the dynamic behaviour of the generator was repetitive when similar thermal states of the machine were considered. However, it is not unusual that the synchronous vibrations of a generator are affected by the effects of a small thermal bow of the shaft induced by the rotor current.

Figure 3 shows the Bode plot of the 1X vibrations measured at bearing #3 during a usual planned coastdown. Therefore, at the beginning of this transient, rotor, casing, pedestals and foundation could be considered in a warm and steady thermal state. In the paper, this coastdown will be denoted Case B. When the rotating speed approached 1850 rpm the amplitude of the 1X vibrations on bearing #3 dropped significantly. Then, in the speed range below 1850 rpm, the levels of these vibration vectors were rather low. At first, this abnormal

behaviour seems to be caused by a serious fault. Anyhow, the evident drop of the vibration amplitude occurred at 1850 rpm has been detected during most of the numerous machine coastdowns. That is, this behaviour showed to be repetitive.

Figure 4 shows the curve of the shaft deceleration occurred during the coastdown (Case B). This curve exhibits a rotating speed dwell, six minutes long, just in a range close to 1850 rpm. During this pause of the machine coastdown the decrease of speed was unimportant. On the contrary, the decrease of temperature in the shaft and copper bars can be assumed to be significant. Unfortunately, no experimental data about these parameters were available.

The safe procedures carried out for the shutdown of the machine composed of the gas-turbine and the generator require the rotating speed dwell occurred during the transient denoted Case B. Therefore, it is possible to suppose that, during usual planned coastdowns, owing to the pause interval, the change in the temperature of the copper bars and shaft induces a change in the thermal bow of the hollow part of shaft. In the present investigation, this variation of the shaft bow has been considered a sort of machine fault as it caused significant and abnormal changes of the shaft vibrations.

This supposition is confirmed by the dynamic behaviour exhibited by the machine during an unplanned emergency shutdown. In the paper, this coastdown will be denoted Case A. In the case of a sudden shutdown it is impossible to effect the rotating speed dwell at 1850 rpm. Therefore, the rotating speed decreases continuously as shown in Figure 4 by the curve of the shaft deceleration associated with this coastdown (Case A). Owing to this, the change in the generator temperature that occurred during the unplanned shutdowns was rather small in comparison with the temperature decrease caused by the usual speed pause that occurred during planned machine shutdowns.

Figure 5 shows a comparison between the 1X vibrations measured at bearing #3, in X direction, during the two transients denoted Case A and Case B. In addition, in the same

figure, the 1X vibrations measured at bearing #3 during a machine runup are illustrated. In the paper, this runup will be denoted Case C.

At the beginning of the planned and unplanned shutdowns that have been considered, the machine thermal state was quite similar. Owing to this, in the speed range from 1850 rpm to 3000 rpm, the 1X vibrations measured at bearing #3 during these two transients were nearly the same (Fig. 5). On the contrary, in the speed range from 130 rpm to 1850 rpm, the 1X vibrations measured during these coastdowns showed significant differences. As said above, the cause of this different dynamic behaviour of the shaft can be ascribed to a different magnitude of a thermal bow which affects the generator rotor.

In the end, in the speed range up to 1800 rpm, the 1X vibrations measured at bearing #3 during the runup, occurred with the machine in a cold thermal state, are rather similar to those measured during planned shutdowns. Conversely, in the speed range from 1850 rpm to 3000 rpm, the 1X vibrations measured during the runup are quite different from those measured during planned and unplanned shutdowns. This different dynamic behaviour is caused by the thermal bow to which the generator rotors are usually affected when operate in the steady thermal state. In fact, owing to different causes, the shaft heating induced by the rotor current can cause an axial asymmetry of the temperature distribution.

In addition to this, Figures 3 and 5 show that, in the speed range near 2600 rpm, the 1X vibration vectors on bearing #3 exhibit a significant decrease of the amplitude as well as a quite evident phase turn. This behaviour was repetitive and was due to a resonance of the pedestal. This natural frequency has been considered in the machine model.

The comparison of the 1X vibrations occurred on bearing #3 during planned and unplanned shutdowns has shown some important differences in the dynamic behaviour of the generator. However, these differences were limited to the portion of shaft near bearing #3. Figures 6 and 7 show the 1X vibrations measured at bearings #1 and #2, respectively, during the two coastdowns denoted Case A and Case B above considered. These figures show that the shaft

vibrations on bearings #1 and #2 were scarcely affected by the presence of a rotating speed dwell during the coastdown, and then by the consequent change in the shaft thermal state. Therefore, these additional information confirm that the drop of the 1X vibration amplitude detected on bearing #3 in the speed range near 1850 rpm was caused by a change in machine excitations located in the part of the shaft near the exciter. That is, in the hollow part of the rotor.

4. FAULT IDENTIFICATION

The cause of the changes in the 1X vibrations of the generator measured during planned and unplanned shutdowns has been considered as a machine fault. The identification of the type of the fault, as well as the identification of its severity its location, has been obtained by applying the model-based technique above described.

This approach requires to estimate the additional 1X vibrations induced by the unknown fault only. The dynamic behaviour of the system was supposed to be linear. Then, the 1X vibration vectors measured during the planned shutdown (Case B) were subtracted from the respective 1X vectors measured during the unplanned shutdown (Case A).

The changes in the shaft excitations associated with the machine fault occurred only in the speed range below 1850 rpm. Therefore, the additional 1X transient vibrations were evaluated only in this range of the rotating speed. Then, these additional vibrations have been analysed by means of the fault identification method.

The experimental transient data were available at many rotating speeds in the range from 130 rpm to 1850 rpm. However, in order to avoid a time consuming analysis, as well as the use of redundant information, only the additional vibrations associated with a limited number of selected rotating speeds were considered. Figure 8 shows the Bode plot of the additional 1X transient vibrations evaluated at bearing #2. In the same figure, the rotating speeds used for the fault identification procedure are indicated.

The preliminary analysis of the transient vibrations of the generator had indicated that the equivalent excitations associated to the fault that had to be identified should be synchronous with the rotating speed. Therefore, bending moments and rotating force vectors were considered. In order to simulate the effects of a shaft bow, two opposite bending moments, having the same amplitude, have been applied to the model of the generator rotor. Extended bows have been modelled by applying the two opposite bending moments to couples of nodes of the FE model whose identification numbers differed significantly. On the contrary, the presence of a local bow has been modelled by applying the bending moments to the ending nodes of two adjacent elements of the FE model of the rotor. For the simulation of the extended bow, increments in the node numbers of 10, 20, 30 and 38 have been considered.

Each analysis has been carried out by shifting the axial location of the bending moments along the shaft model. In addition, each analysis has provided an estimate of the global residue ε_1 and the magnitude and phase of the moments, as well.

Figure 9 shows the relationship between the global residue ε_1 and the location of the bending moments. In this figure, the residue associated with each couple of bending moments has been plotted along the shaft in the location that corresponds to the mid-span of the distance between the two nodes to which the moments were applied.

In Figure 9, the locations of the bending moments associated with the minimum residue of each analysis have been shown together with the value of this residue.

Moreover, the results of the analysis by which a local bow of the shaft has been simulated are shown in Figure 10.

Shaft bows whose extension was rather large have caused very low values of the global residue ε_1. On the contrary, the minimum residue associated with a local bow is significantly higher than the residues obtained with the extended bows.

The best results obtained with the maximum extension of the shaft bow are associated with two opposite bending moments applied to nodes of the rotor model that are very close to the

ends of the hollow part of the shaft. That is, the locations of these moments are very close to the sections at which the copper bar are constrained to the rotor. Therefore, when shaft and copper bars were subjected to a significant thermal transient, e.g. during planned coastdowns, the hollow part of the generator rotor could be subjected to a thermal bow. Then, the identification of two equivalent bending moments applied in the shaft locations above described corresponds to a likely fault.

The values of the minimum residues associated with some shaft bows of shorter extension are very similar to the residue obtained by applying the moments to the ends of the hollow part of the shaft. However, these results are not in contrast each other because the location of one of the two bending moments is always very close to the inboard cross-section at which the copper bars are constrained to the shaft.

Although it was rather improbable that the effects of the machine fault could be simulated by means of a local unbalance, a fault identification in which a synchronous rotating force has been considered was carried out. Figure 10 shows the relationship between the global residue ε_1 and the location of the unbalance mass. In this case the minimum residue is associated to an unbalance located just at the end of the shaft, that is on the flange towards the connection with the steam turbine. The minimum residue obtained with this analysis is significantly higher than the minimum residues associated with the identified extended bows.

The minimum residues estimated with each identification procedure are summarised in Table 1 while the magnitude and phase of the respective equivalent excitations are shown in Table 2.

The equivalent excitations that simulate the effects of the machine fault in the best possible way have been identified using the additional transient vibrations associated with a limited number of rotating speeds of the generator. An additional validation of these results was carried out by evaluating the machine response, induced by the identified fault, at every rotating speed at which the additional 1X transient vibrations were available.

Figures 11 and 12 show the comparison between the experimental additional vibrations at bearings #2 and #3 and the respective numerical results provided by the simulating model. The curve fitting is very good over the complete speed range from 400 rpm to 1850 rpm.

Figure 13 shows the comparison between the experimental additional vibrations at bearing #1 and the respective numerical results. Also in this case, the experimental curves of the phase of the 1X vibrations are fitted in a satisfactory way by the numerical results. On the contrary, the amplitudes of the experimental vibrations are underestimated by the numerical response evaluated using the identified bending moments.

However, it is important to consider that the levels of the 1X vibrations induced by the fault on bearing #1 are rather low. Therefore, the evaluation of the additional vibrations on this support can be affected by more important relative errors. In conclusion, Figures 11-13 show that the absolute values of the fitting errors are rather small for all the measurement points of the generator vibrations.

5. RESIDUE ANALYSIS

As said above, the machine response induced by the identified fault has been evaluated at every rotating speed at which the additional 1X transient vibrations were available. This analysis has allowed the estimation of a further residue, ε_2, to be carried out. In this case, the errors between experimental vibration data and the respective numerical results have been evaluated for a larger number of rotating speed values, in comparison with the identification procedure.

The value of the global residue ε_2 was 0.4035. This value is very close to the minimum value of the residue ε_1 (0.3782) provided by the fault identification procedure in which the vibrations data associated with only nine rotating speeds have been considered. The accordance between the residues ε_1 and ε_2 confirms the reliability of the results provided by the fault identification as well as the robustness of the method.

In addition, the relationship between the residue ε_2 and the rotating speed has been analysed. In Figure 14 the residues ε_ω, evaluated with the identified bending moments, are plotted against the rotating speed. In general, the values of these residues are rather low over the complete speed range from 400 rpm to 1850 rpm. Only a small increase occurs in the speed range near the first balance resonance of the shaft.

The numerical response caused by the identified bending moments has been evaluated at the degrees of freedom associated with the horizontal and vertical lateral vibrations of each support of the generator. Then, a further analysis allowed the residue, ε_{dof}, associated with each degree of freedom to be evaluated. The estimates of these partial residues are shown in Figure 15. It is possible to note that the residues associated with the degrees of freedom of bearing #3 are very low, as confirmed by the diagrams shown in Figure 12. The residues ε_{dof} associated with bearings #1 and #2 are higher but, as said above, it is important to consider that the 1X additional vibrations evaluated at these bearings were rather low. Therefore, in this case, even little absolute errors in the fitting of the experimental data can cause a significant value of the residue.

In fact, the residues are estimates of the relative errors of the fault identification procedure. Therefore, this analysis of the residues has been integrated with the analysis of the absolute error between the experimental vibration data and the respective numerical results obtained with the identified fault. In Figure 16 the absolute error, evaluated considering the responses at the degrees of freedom of the three supports of the generator, is plotted against the rotating speed.

Also in this case, the values of this curve are rather low over the complete speed range from 400 rpm to 1850 rpm. Only a small increase occurs in the speed range near the first balance resonance of the shaft where a maximum value of only 12 μm pk-pk is reached.

In the end, the analysis of the residues has been integrated with a correlation analysis between numerical and experimental vibration data. Figure 17 shows the results of this investigation.

The dashed line plotted in Figure 17 has been obtained with a linear regression analysis of the data. The two thick lines, that are parallel to the regression straight line, are plotted at a distance equal to two times the standard deviation σ_r of the regression errors (σ_r = 2.9 μm). In accordance with the results above described, the larger dispersion of the regression errors is associated with the vibrations that show the lowest amplitudes. The MAC index was 0.97958: that is, it was very close to the ideal unity value. Some results of a statistical analysis of the residues are shown in Table 3.

6. RESULT VALIDATION

A further validation of the results provided by the fault identification above described has been carried out by means of the analysis of the experimental transient response of the generator measured in occasion of a special case history.

The condition monitoring system collected the transient vibration data during a partial coastdown of the power unit at the end of which the rotating speed of the machine was increased up to the operating speed value and, finally, the unit was put in service once again. Figure 18 shows the trending of the rotating speed of the generator during this transient. At first, the speed decreased from 3000 rpm to 1780 rpm. After a pause of nearly six minutes, the rotating speed was increased again up to 3000 rpm. During this transient and, in particular, during the pause of the machine deceleration, the shaft and the copper bars placed in the hollow of the rotor were subjected to a cooling that was very similar to the thermal transient that occurs during the usual planned shutdowns of the unit.

Figure 19 shows the Bode plot of the 1X vibrations measured at bearing #3 of the generator during this partial coastdown and the subsequent restart. The 1X vibrations at bearing #3 were significantly affected by the machine thermal state. In fact, during the speed dwell the amplitude of the 1X vectors decreased. When the machine was restarted, the 1X vibrations at bearing #3 exhibited very different values in comparison with the vibration data collected

during the previous coastdown, at the respective rotating speed. By considering the speed range from 1800 rpm to 3000 rpm only, this dynamic behaviour was very similar to those one occurred during the two coastdowns above analysed (Cases A and B). Therefore, it is possible to suppose that the speed dwell occurred at the end of the partial coastdown caused a change in the shaft bow. In turn, this phenomenon induced changes in the 1X vibrations of the rotor.

The additional transient vibrations which can be ascribed to the effects of the changes in the thermal bow of the generator were evaluated. That is, the 1X vibration vectors measured during the partial runup (machine restart) were subtracted from the respective 1X vectors measured during the partial coastdown.

Then, the simulating model of the generator has been used to evaluate the vibrations induced by the same bending moments that had been estimated with the previous identification procedure. It is important to remark that these bending moments had been identified by analysing additional transient vibrations different from those considered in the present case study. In addition, the bending moments had been identified by analysing vibration data collected in the speed range from 400 rpm to 1850 rpm. On the contrary, in the present investigation, the additional transient vibrations of the generator have been analysed in the speed range from 1800 rpm to 3000 rpm. However, in this analysis, the same bending moments previously identified have been used.

Figure 20 shows the comparison between the experimental additional vibrations at bearing #3 and the respective numerical results provided by the simulating model. The accordance between experimental data and numerical results is satisfactory over the complete speed range from 1800 rpm to 3000 rpm. It is important to consider that in the rotating speed range near 2600 rpm the dynamic behaviour of the shaft at bearing #3 is affected also by the effects of a resonance of the foundation structure. Nevertheless, the vibration data provided by the model fit the experimental curves with a satisfactory accuracy.

This investigation allowed an estimate of the residue ε_2 to be evaluated. The value of this residue was 0.7077.

In conclusion, the results obtained with this further analysis are satisfactory and confirm the reliability of the type of fault that has been identified as well as the accuracy of the estimate of magnitude, phase and location of the equivalent bending moments which have been used to model the thermal bow of the generator shaft.

7. CONCLUSIONS

The transient vibrations of a generator rotor that was affected by a thermal bow has been analysed. The shaft bow was caused by an axial asymmetry of the temperature distribution of the rotor induced by the electrical current that flows in the copper conductors. Therefore, the severity of the shaft bow depended on the generator thermal state.

During the usual planned shutdowns of the power unit a rotating speed dwell, six minutes long, occurred. During this pause of the coastdown the machine was subjected to a thermal transient. Owing to the cooling of the shaft and the copper bars placed in the hollow part of the generator rotor, during usual machine coastdowns, the severity of the shaft bow changed significantly. This caused important changes in the generator synchronous vibrations. This phenomenon has been considered a machine fault that could be modelled with a couple of opposite bending moments applied to suitable locations of the shaft.

The magnitude, phase and location of these equivalent excitations have been estimated with a model-based identification technique. The theoretical response of the system induced by the identified bending moments has been evaluated with the simulating model and compared with the respective experimental transient vibrations. The errors between numerical results and experimental data showed to be rather low, especially for the measurement points at which the shaft bow caused the highest vibration amplitudes.

In the paper, the results obtained by considering different bow extensions are shown and discussed. The best fitting between experimental vibration data and numerical results has been obtained by applying two opposite bending moments at the cross-sections of the generator at which the copper bars, placed in the hollow part of the shaft, are constrained. Therefore, the identified fault is very likely.

In addition, the results obtained with the identification technique by assuming that the fault was caused by a local unbalance have been compared with the results obtained by modelling the fault with two opposite bending moments. This analysis has confirmed very clearly that the generator was affected by a shaft thermal bow rather than by an unbalance.

The fault identification has been integrated with a statistical analysis of the errors between experimental data and numerical results provided by the simulating model. In the paper, the results of this analysis are shown and discussed.

This study of the errors enables some measures of the accuracy of the fault identification to be obtained.

This investigation proved that the model-based technique developed to identify faults and malfunctions in rotating machinery is able to provide successful results. Therefore, this approach can be very useful for diagnostic purposes.

ACKNOWLEDGEMENTS

This work is partially funded by the MIUR (Italian Ministry for the University and Scientific Research) Cofinanziamento "TECNICHE DI IDENTIFICAZIONE DI MALFUNZIONAMENTI DI SISTEMI MECCANICI BASATE SULL'ANALISI DEL COMPORTAMENTO DINAMICO" for the year 2001.

REFERENCES

1. R. Markert, R. Platz and M. Seidler 2000 Proc. of ISROMAC-8, Vol. II, ISBN 0-9652469-9-X, Texas A&M University, 901-907. Model Based Fault Identification in Rotor Systems by Least Squares Fitting.
2. R. Platz and R. Markert 2001 Proc. of the 4th Int. Conference on Acoustical and Vibratory Surveillance Methods and Diagnostic Techniques, October 16-18, 2001, Compiègne (France), 435-446. Fault Models for On-line Identification of Malfunctions in Rotor Systems.
3. N. Bachschmid, P. Pennacchi P. and A. Vania 2002 Journal of Sound and Vibration, vol. 254, no. 2, pp. 327-366. Identification of Multiple Faults in Rotor Systems.
4. N. Bachschmid, P. Pennacchi, E. Tanzi and A. Vania 2000, Journal of the Brazilian Society of Mechanical Sciences, Vol. XXII, No 3, ISSN 0100-7386, 423-442. Accuracy of Modelling and Identification of Malfunctions in Rotor Systems: Experimental Results.
5. N. Bachschmid, P. Pennacchi and A. Vania 2001 Condition Monitoring and Diagnostic Engineering Management, A. G. Starr, B. K. N. Rao Editors, Elsevier Science Ltd., Oxford, 2001, ISBN 0-08-044036-3, 663-671. Experimental Results in Simultaneous Identification of Multiple Faults in Rotor Systems.
6. P. Pennacchi and A. Vania 2001 Condition Monitoring and Diagnostic Engineering Management, A. G. Starr, B. K. N. Rao Editors, Elsevier Science Ltd., Oxford, 2001, ISBN 0-08-044036-3, 873-880. Measures of Accuracy of Model Based Diagnosis of Faults in Rotormachinery.
7. D. J. Ewins 1984 Modal Testing: Theory and Practice, Research Studies Press, Letchworth.

NOMENCLATURE

$\mathbf{D}$ damping matrix;

$\mathbf{F}_n$ n^{th} force vector harmonic component due to faults;

$\mathbf{H}_n$ transfer matrix;

$\mathbf{H}_m$ partition of $\mathbf{H}_n$ for the nodes corresponding to measuring points;

$\mathbf{H}_r$ partition of $\mathbf{H}_n$ for the nodes not corresponding to measuring points;

$\mathbf{K}$ stiffness matrix;

$\mathbf{M}$ mass matrix;

n number of the harmonic component;

$\mathbf{X}_1$ real vector composed by the real and the imaginary part of theoretical vibrations;

$\mathbf{X}_2$ real vector composed by the real and the imaginary part of experimental vibrations;

$\mathbf{X}_{ex}$ experimental transient vibrations;

$\mathbf{X}_m$ partition of $\mathbf{X}_n$ for the nodes not corresponding to measuring points;

$\mathbf{X}_r$ partition of $\mathbf{X}_n$ for the nodes corresponding to measuring points;

$\mathbf{X}_n$ n^{th} vibration harmonic component;

δ difference between calculated and measured vibrations;

ε_1 relative residue calculated for a subset of the available measures;

ε_2 relative calculated for all the available measures;

ε_{dof} relative calculated for each measured degree of freedom;

ε_ω relative calculated for each rotating speed;

Ω rotating speed, frequency;

TABLES

Table 1. Global residue.

	Extended bow				Local bow	Unbalance
Bow extension	38 nodes	30 nodes	20 nodes	10 nodes	2 nodes	
Residue ε_1	0.3782	0.3766	0.3860	0.4199	0.4251	0.7223

Table 2. Identified bending moments.

		Extended bow				Local bow
	Bow extension	38 nodes	30 nodes	20 nodes	10 nodes	2 nodes
Bending moments	Amplitude [Nm]	1504	1889	2648	4372	7247
	Phase [degrees]	270° / 90°	269° / 89°	271° / 91°	271° / 91°	273° / 93°

Table 3. Results of a statistical analysis of residues.

Global residue	Global residue	Mean value of residues $\varepsilon_{\mathrm{dof}}$	Standard deviation of residues $\varepsilon_{\mathrm{dof}}$	Mean value of residues ε_{ω}	Standard deviation of residues ε_{ω}
ε_1	ε_2	$\mu_{\varepsilon\,\mathrm{dof}}$	$\sigma_{\varepsilon\,\mathrm{dof}}$	$\mu_{\varepsilon\,\omega}$	$\sigma_{\varepsilon\,\omega}$
0.3782	0.4035	0.5835	0.3805	0.3599	0.1043

FIGURE CAPTIONS

Figure 1. Rotor train diagram.

Figure 2. Finite Element model of the generator shaft.

Figure 3. Bode plot of the 1X vibrations measured at bearing #3 during a normal planned coastdown.
Thick line: X direction (45°R). Fine line: Y direction (45°L).

Figure 4. Generator rotating speed vs. time, during an unplanned shutdown (Case A) and a normal planned shutdown (Case B).

Figure 5. Bode plot of the 1X vibrations measured at bearing #3, in the X direction (45°R), during an unplanned shutdown (Case A), a planned shutdown (Case B) and a runup (Case C).
Dashed line: Case A. Fine line: Case B. Dotted line: Case C.

Figure 6. Bode plot of the 1X vibrations measured at bearing #1, in X and Y direction, during the unplanned (Case A) and planned (Case B) shutdowns. Dotted line: Case A, X direction (45°R). Dashed line: Case A, Y direction (45°L). Thick line: Case B, X direction (45°R). Fine line: Case B, Y direction (45°L).

Figure 7. Bode plot of the 1X vibrations measured at bearing #2, in X and Y direction, during the unplanned (Case A) and planned (Case B) shutdowns. Dotted line: Case A, X direction (45°R). Dashed line: Case A, Y direction (45°L). Thick line: Case B, X direction (45°R). Fine line: Case B, Y direction (45°L).

Figure 8. Bode plot of the additional 1X experimental vibrations evaluated at bearing #2 and rotating speeds considered for the fault identification procedure. Thick line: X direction (45°R). Fine line: Y direction (45°L).

Figure 9. Relationship between the global residue ε_1 and the bending moment locations. Case study: extended bow simulated with an increment of 10, 20, 30, 38 nodes between the locations of the two opposite bending moments.

Figure 10. Relationship between the global residue ε_1 and equivalent excitation locations. Case study: local bow simulated with an increment of 2 nodes between the locations of the two opposite bending moments local unbalance.

Figure 11. Additional vibrations (1X) at bearing #2. Comparison between experimental vibrations and numerical results obtained with the identified fault. Dotted line: horizontal

experimental vibrations. Dashed line: vertical experimental vibrations. Thick line: horizontal theoretical vibrations. Fine line: vertical theoretical vibrations.

Figure 12. Additional vibrations (1X) at bearing #3. Comparison between experimental vibrations and numerical results obtained with the identified fault. Dotted line: horizontal experimental vibrations. Dashed line: vertical experimental vibrations. Thick line: horizontal theoretical vibrations. Fine line: vertical theoretical vibrations.

Figure 13. Additional vibrations (1X) at bearing #1. Comparison between experimental vibrations and numerical results obtained with the identified fault. Dotted line: horizontal experimental vibrations. Dashed line: vertical experimental vibrations. Thick line: horizontal theoretical vibrations. Fine line: vertical theoretical vibrations.

Figure 14. Global residue ε_2 vs. rotating speed.

Figure 15. Residues ε_{dof} evaluated for each degree of freedom associated with the lateral vibrations of the generator supports.

Figure 16. Absolute error vs. rotating speed.

Figure 17. Correlation analysis between numerical and experimental vibration data.

Figure 18. Generator rotating speed vs. time, during the partial coastdown and the subsequent runup.

Figure 19. Bode plot of the 1X vibrations measured at bearing #3, in X and Y direction, during the partial coastdown and the subsequent runup (Case D). Thick line: X direction (45°R). Fine line: Y direction (45°L).

Figure 20. Additional vibrations (1X) at bearing #3. Comparison between experimental vibrations and numerical results obtained with the identified fault. Dotted line: horizontal experimental vibrations. Dashed line: vertical experimental vibrations. Thick line: horizontal theoretical vibrations. Fine line: vertical theoretical vibrations.

FIGURES

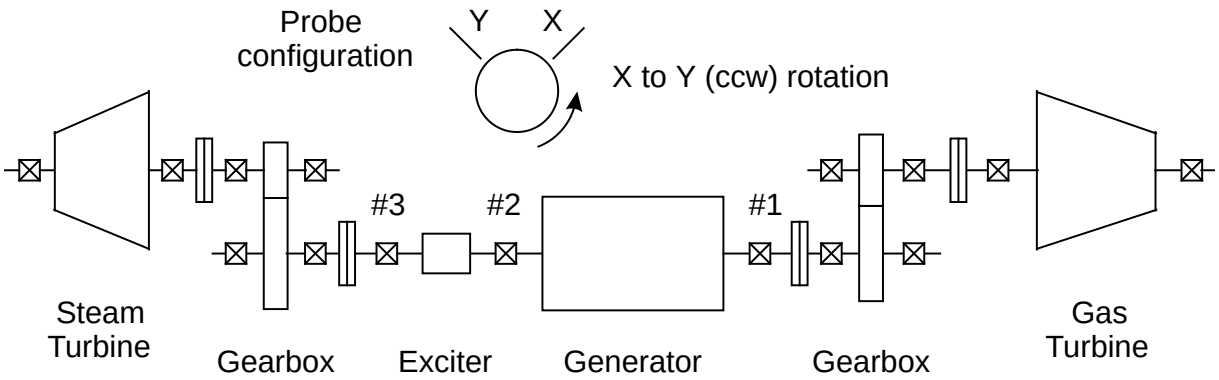

Figure 1. Rotor train diagram.

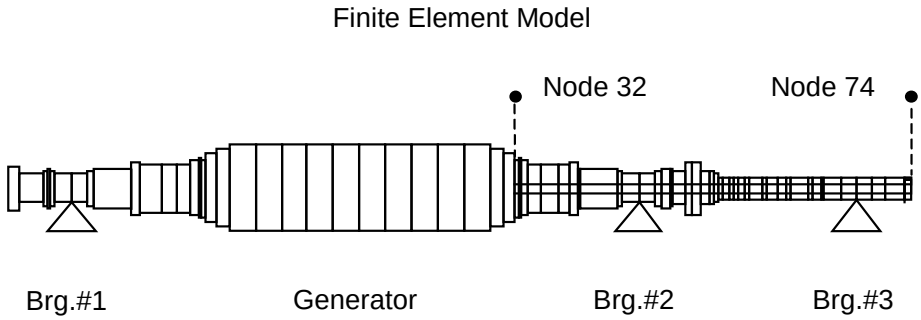

Figure 2. Finite Element model of the generator shaft.

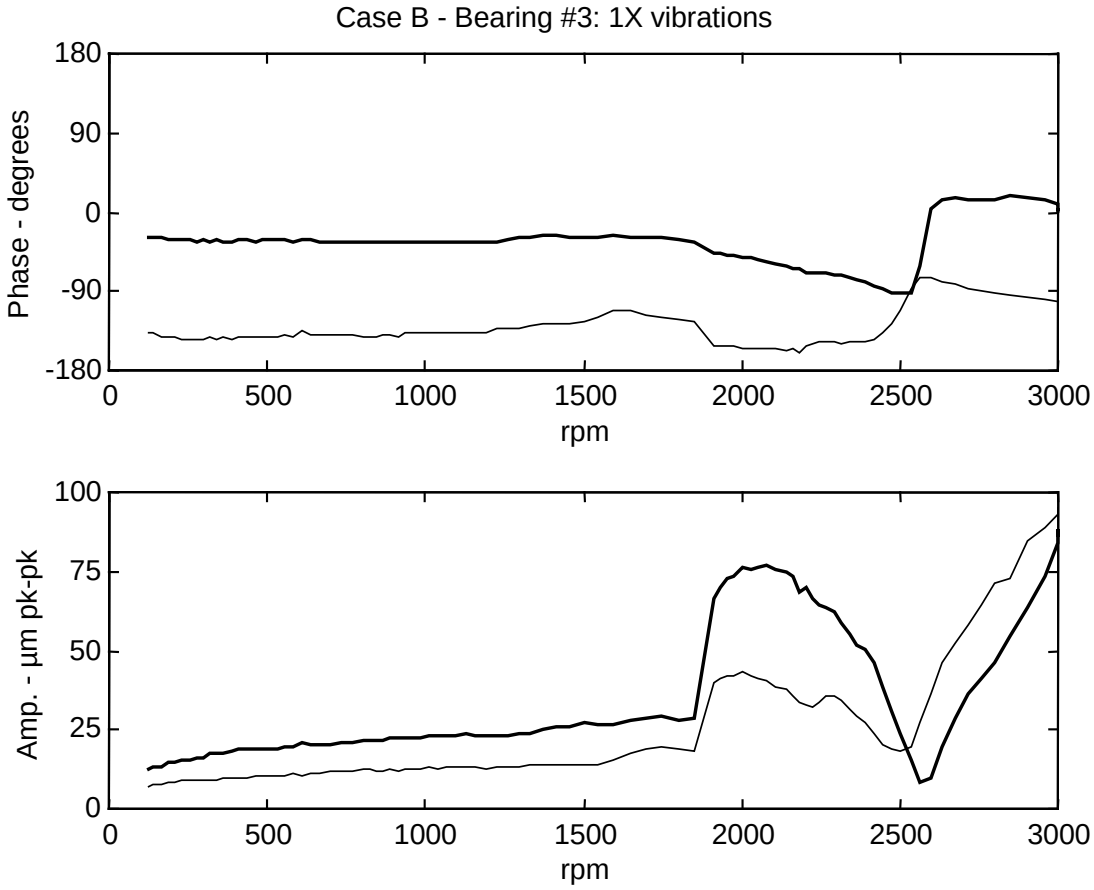

Figure 3. Bode plot of the 1X vibrations measured at bearing #3 during a normal planned coastdown.
Thick line: X direction (45°R). Fine line: Y direction (45°L).

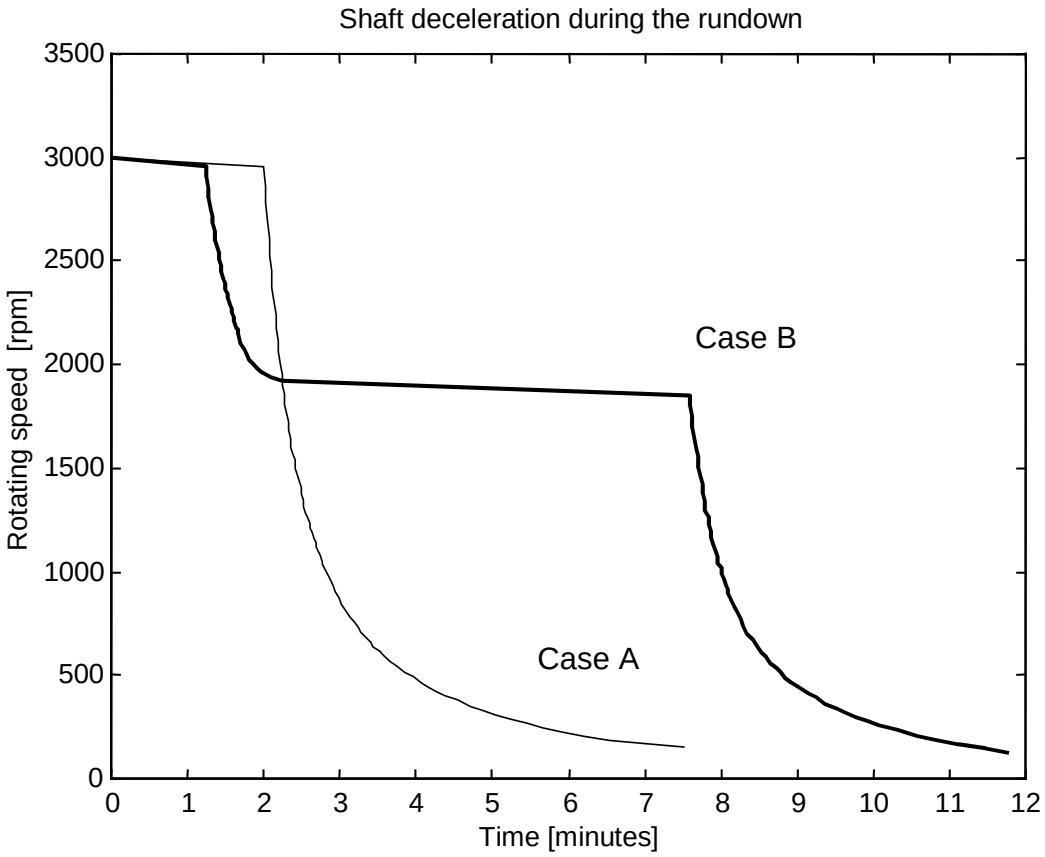

Figure 4. Generator rotating speed vs. time, during an unplanned shutdown (Case A) and a normal planned shutdown (Case B).

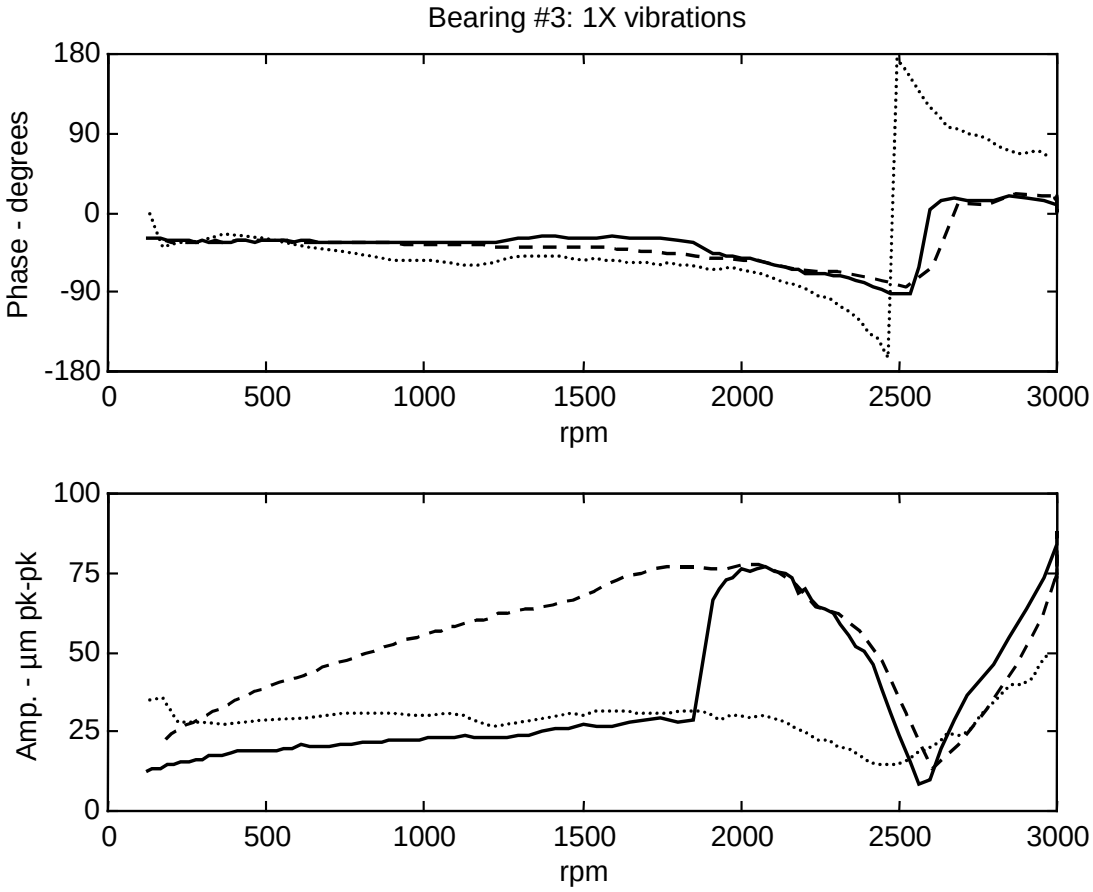

Figure 5. Bode plot of the 1X vibrations measured at bearing #3, in the X direction (45°R), during an unplanned shutdown (Case A), a planned shutdown (Case B) and a runup (Case C). Dashed line: Case A. Fine line: Case B. Dotted line: Case C.

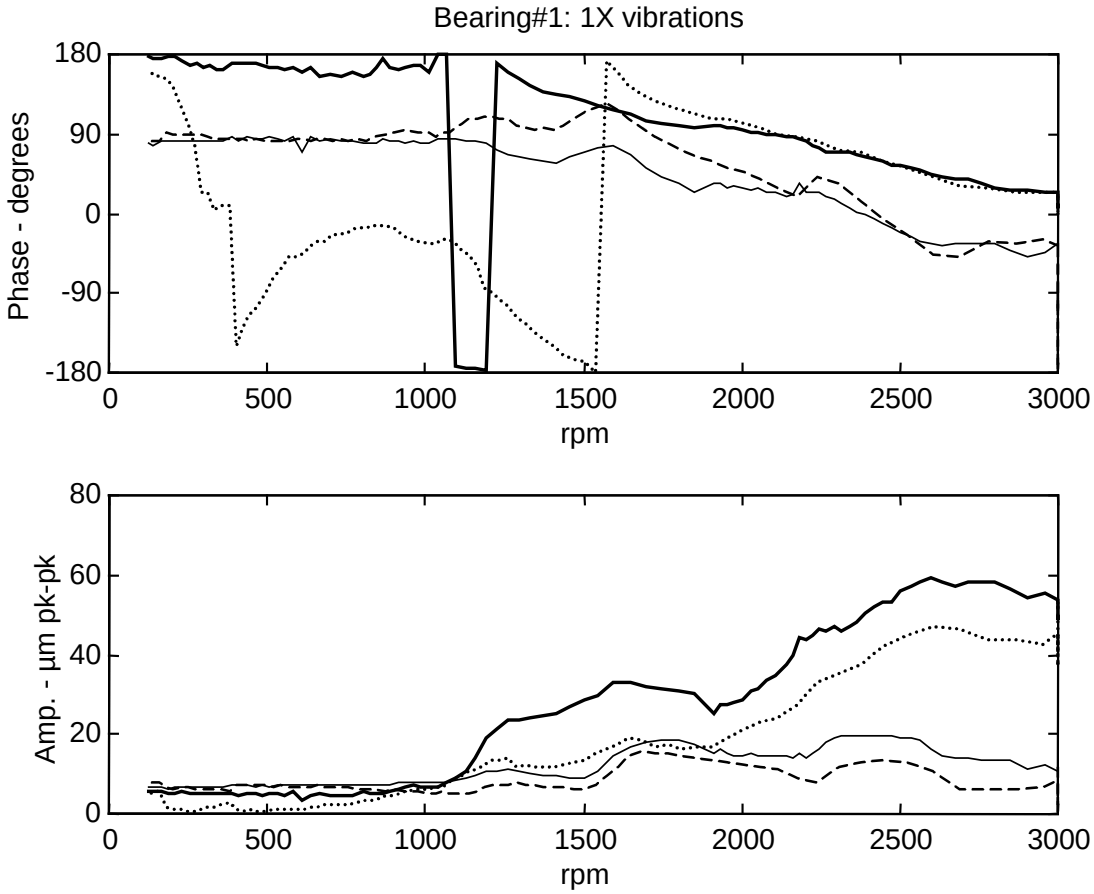

Figure 6. Bode plot of the 1X vibrations measured at bearing #1, in X and Y direction, during the unplanned (Case A) and planned (Case B) shutdowns. Dotted line: Case A, X direction (45°R). Dashed line: Case A, Y direction (45°L). Thick line: Case B, X direction (45°R). Fine line: Case B, Y direction (45°L).

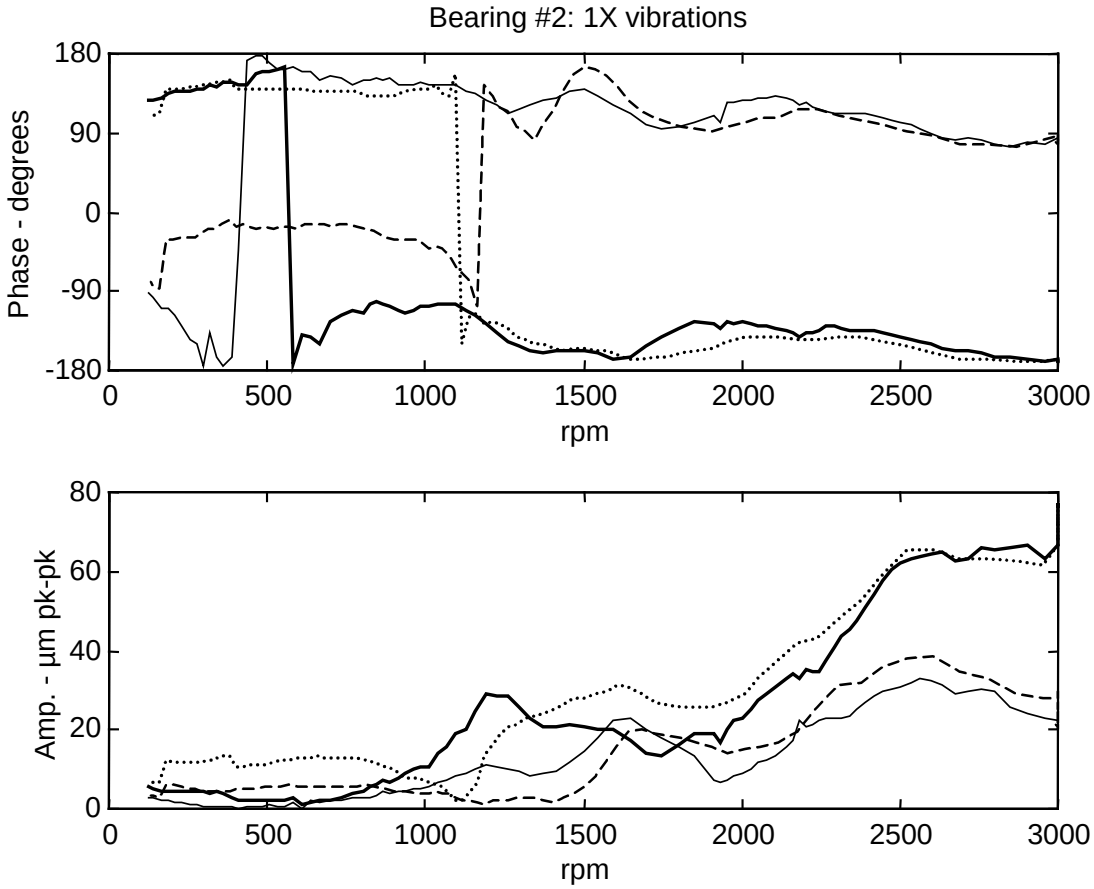

Figure 7. Bode plot of the 1X vibrations measured at bearing #2, in X and Y direction, during the unplanned (Case A) and planned (Case B) shutdowns. Dotted line: Case A, X direction (45°R). Dashed line: Case A, Y direction (45°L). Thick line: Case B, X direction (45°R). Fine line: Case B, Y direction (45°L).

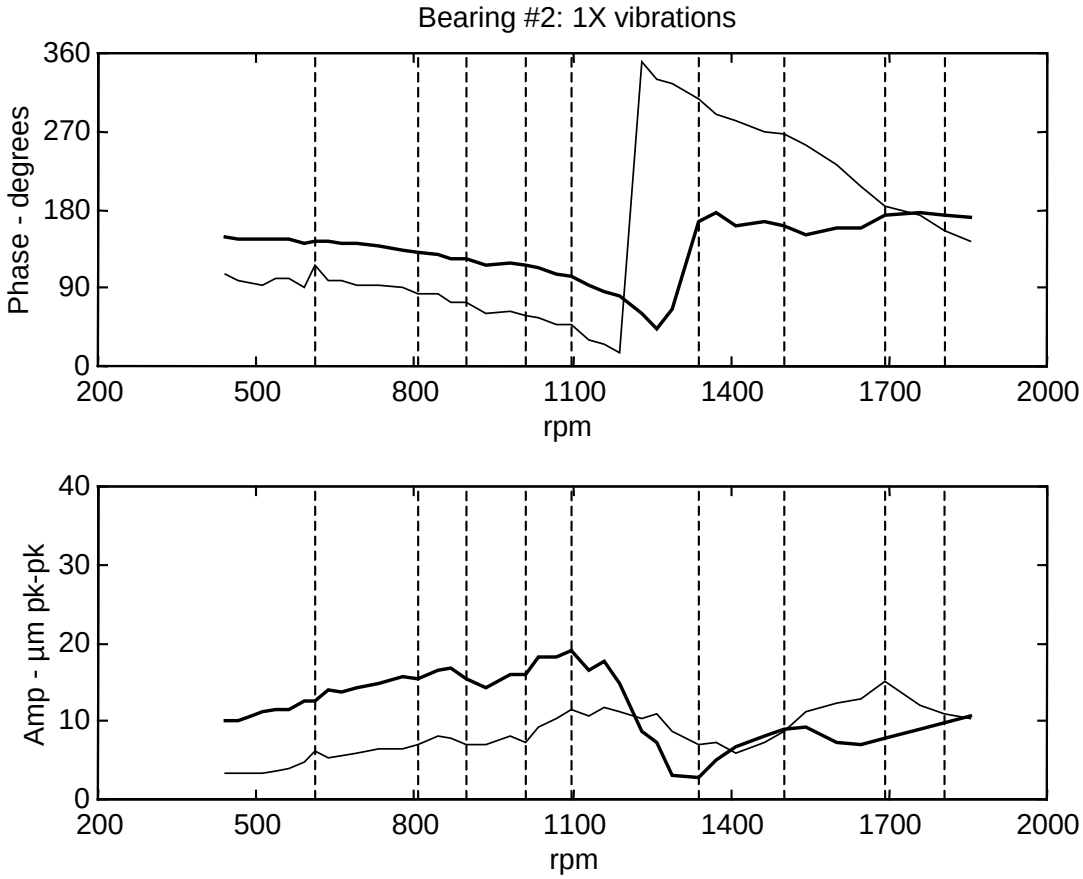

Figure 8. Bode plot of the additional 1X experimental vibrations evaluated at bearing #2 and rotating speeds considered for the fault identification procedure. Thick line: X direction (45°R). Fine line: Y direction (45°L).

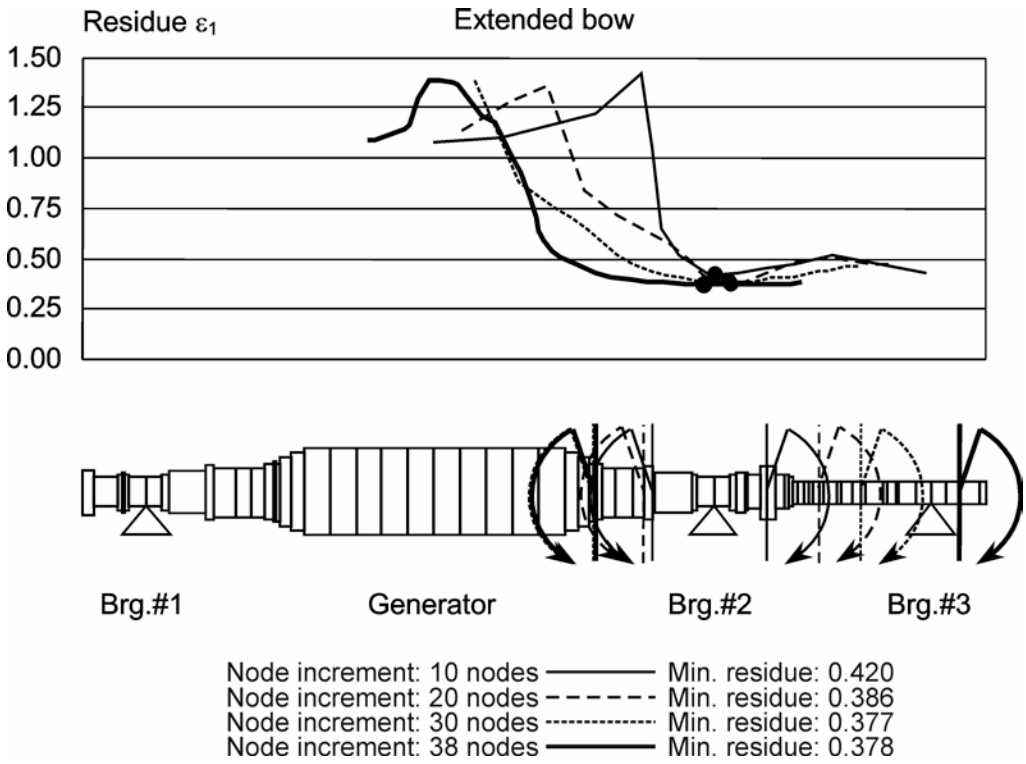

Figure 9. Relationship between the global residue ε_1 and the bending moment locations. Case study: extended bow simulated with an increment of 10, 20, 30, 38 nodes between the locations of the two opposite bending moments.

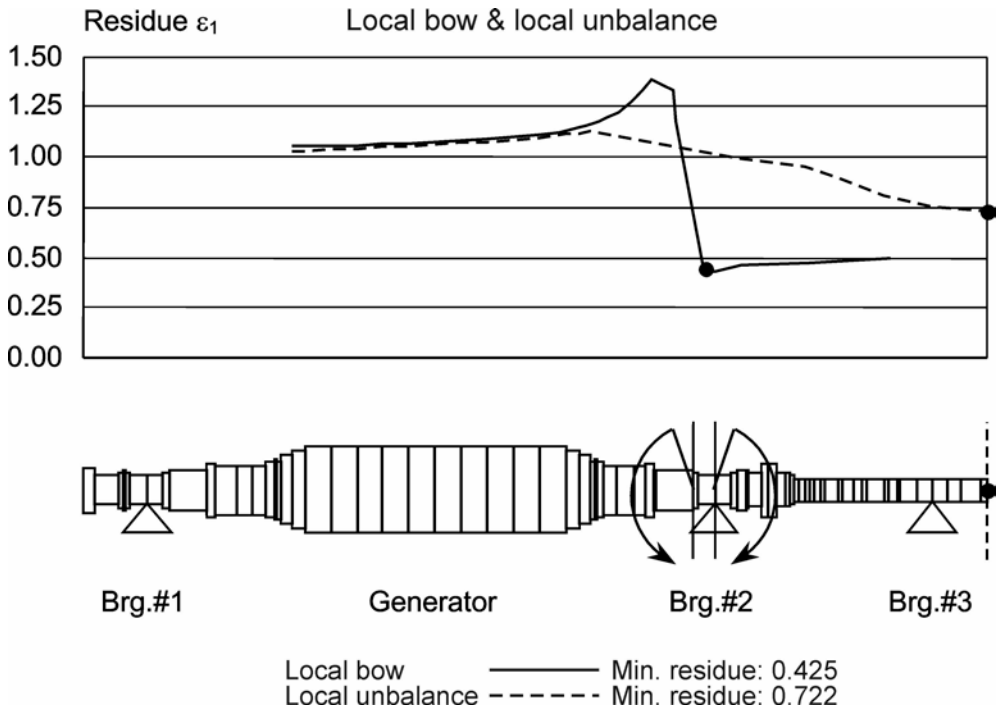

Figure 10. Relationship between the global residue ε_1 and equivalent excitation locations. Case study: local bow simulated with an increment of 2 nodes between the locations of the two opposite bending moments local unbalance.

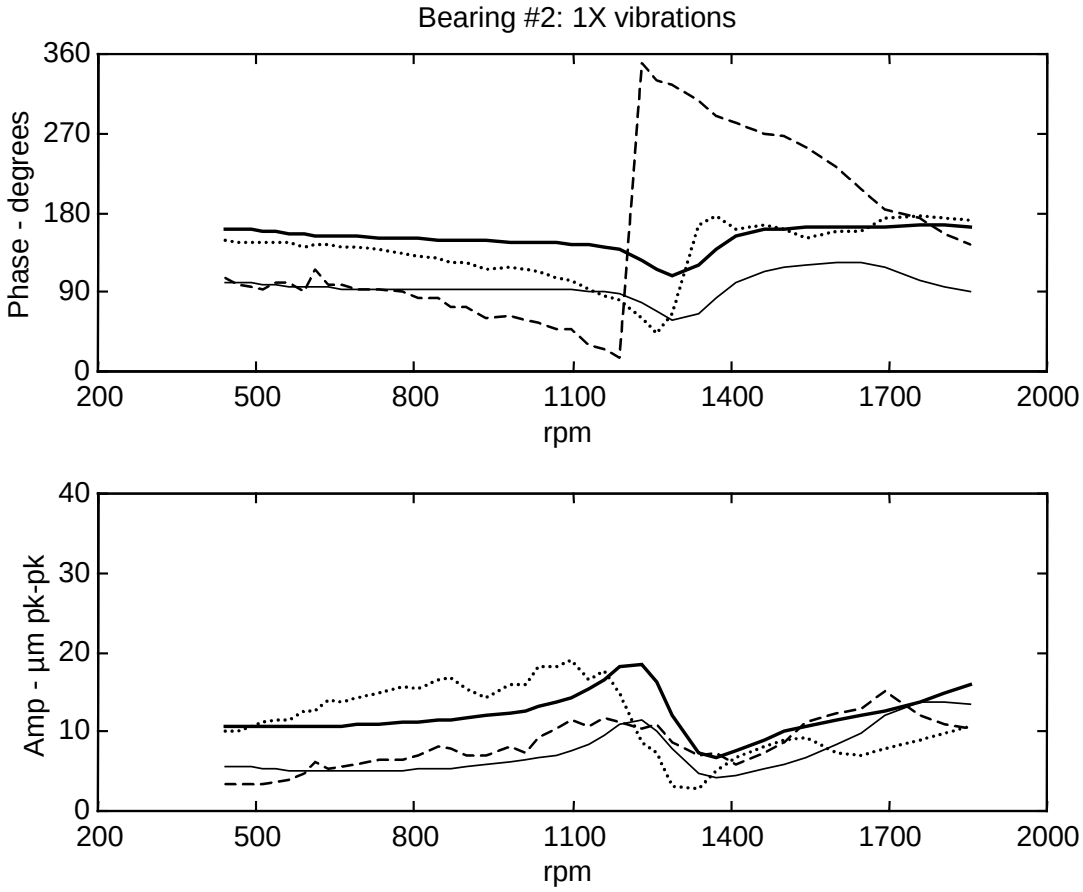

Figure 11. Additional vibrations (1X) at bearing #2. Comparison between experimental vibrations and numerical results obtained with the identified fault. Dotted line: horizontal experimental vibrations. Dashed line: vertical experimental vibrations. Thick line: horizontal theoretical vibrations. Fine line: vertical theoretical vibrations.

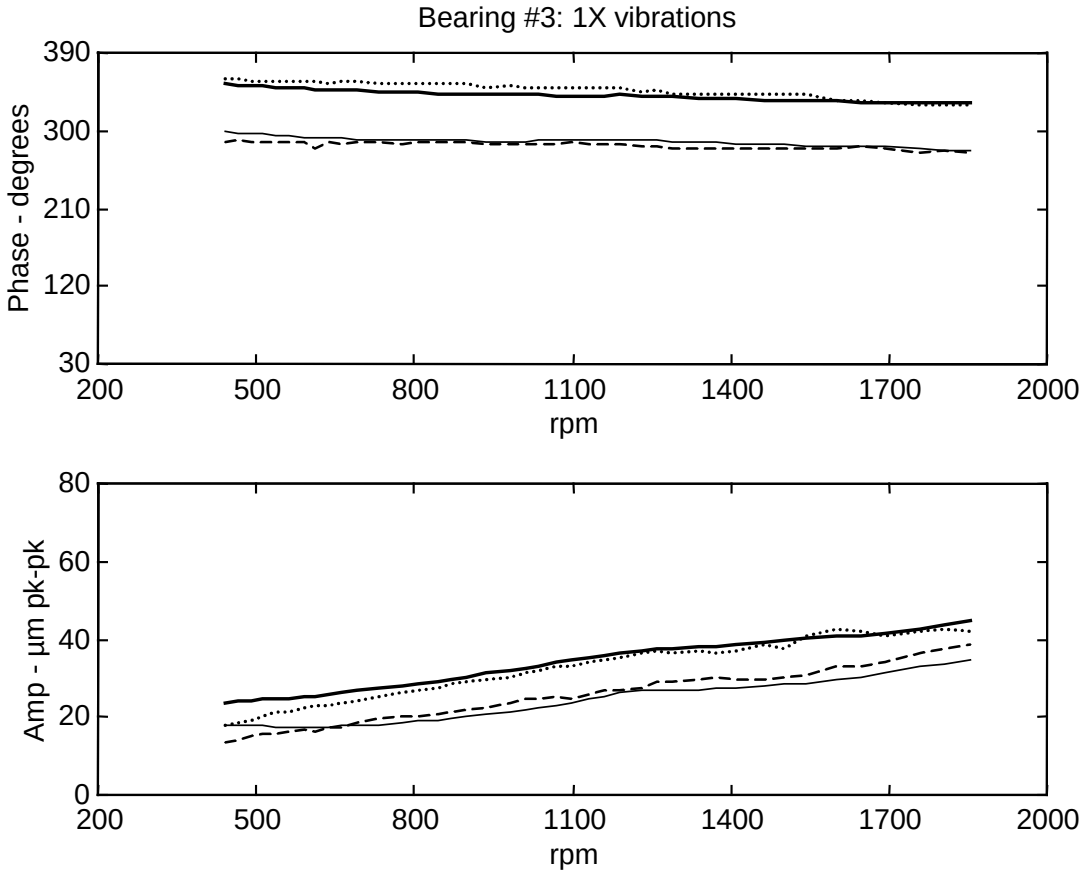

Figure 12. Additional vibrations (1X) at bearing #3. Comparison between experimental vibrations and numerical results obtained with the identified fault. Dotted line: horizontal experimental vibrations. Dashed line: vertical experimental vibrations. Thick line: horizontal theoretical vibrations. Fine line: vertical theoretical vibrations.

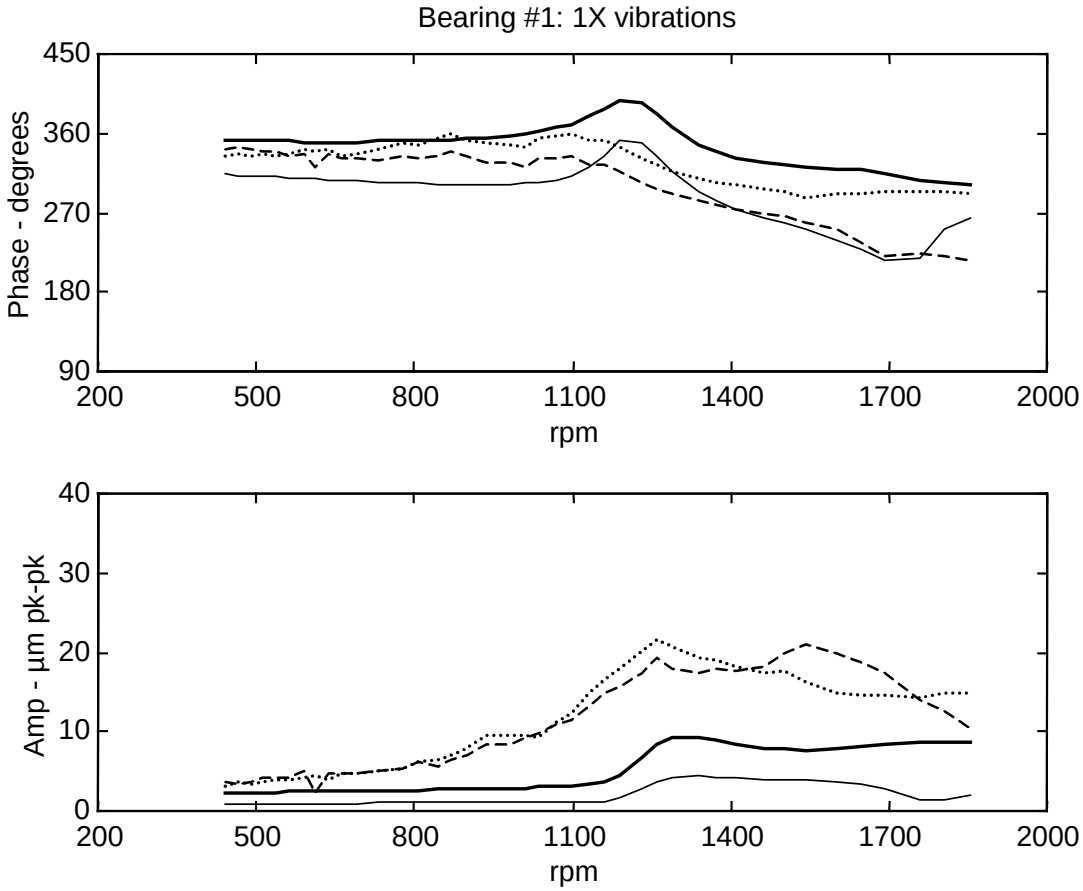

Figure 13. Additional vibrations (1X) at bearing #1. Comparison between experimental vibrations and numerical results obtained with the identified fault. Dotted line: horizontal experimental vibrations. Dashed line: vertical experimental vibrations. Thick line: horizontal theoretical vibrations. Fine line: vertical theoretical vibrations.

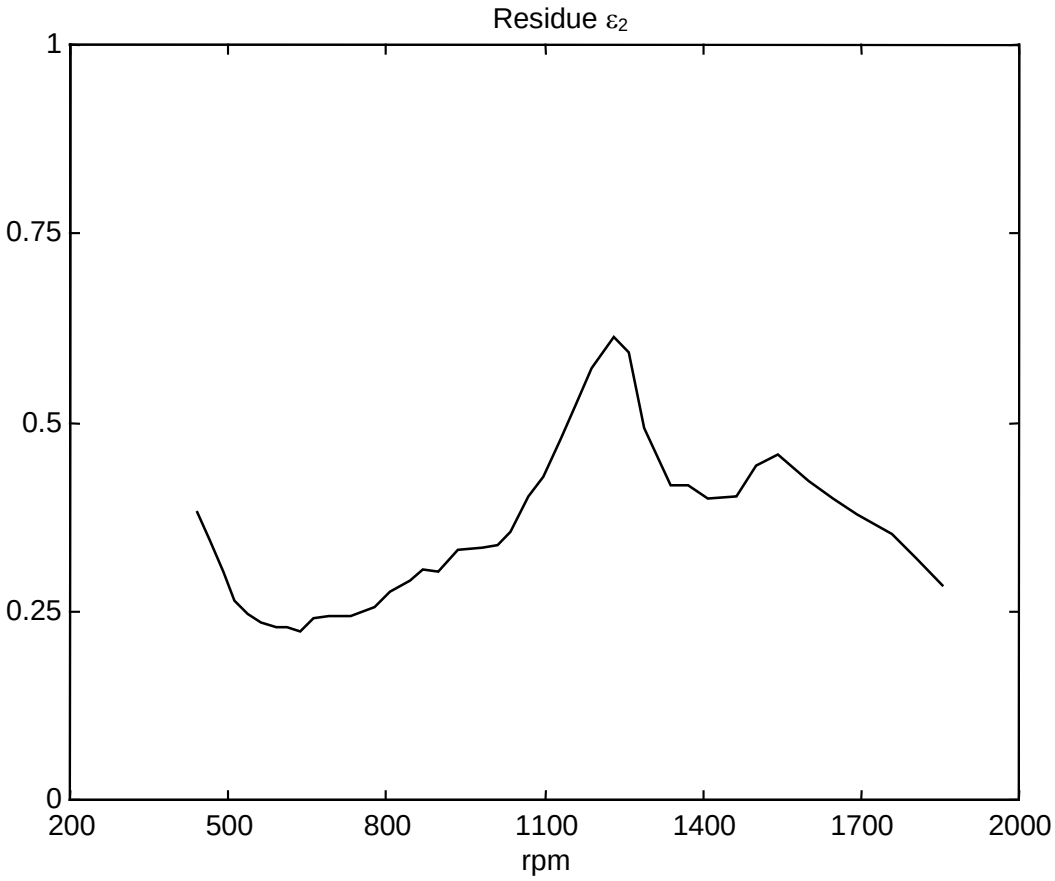

Figure 14. Global residue ε_2 vs. rotating speed.

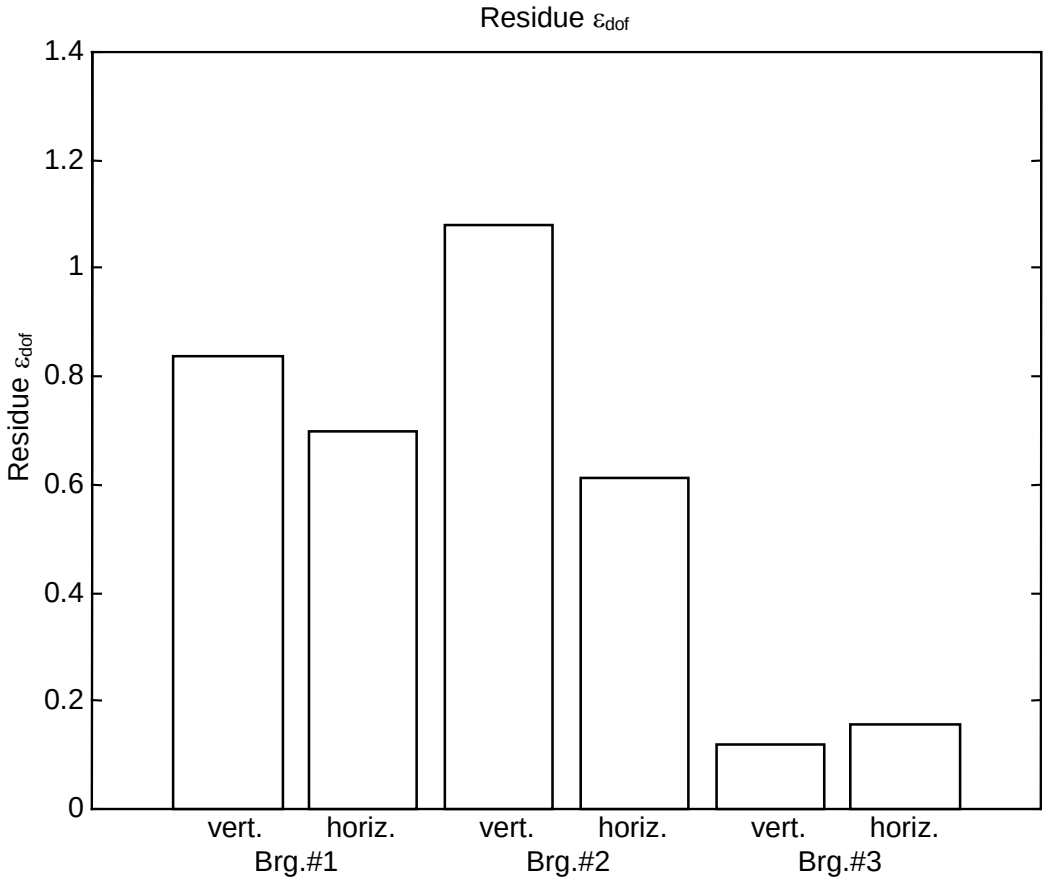

Figure 15. Residues ε_{dof} evaluated for each degree of freedom associated with the lateral vibrations of the generator supports.

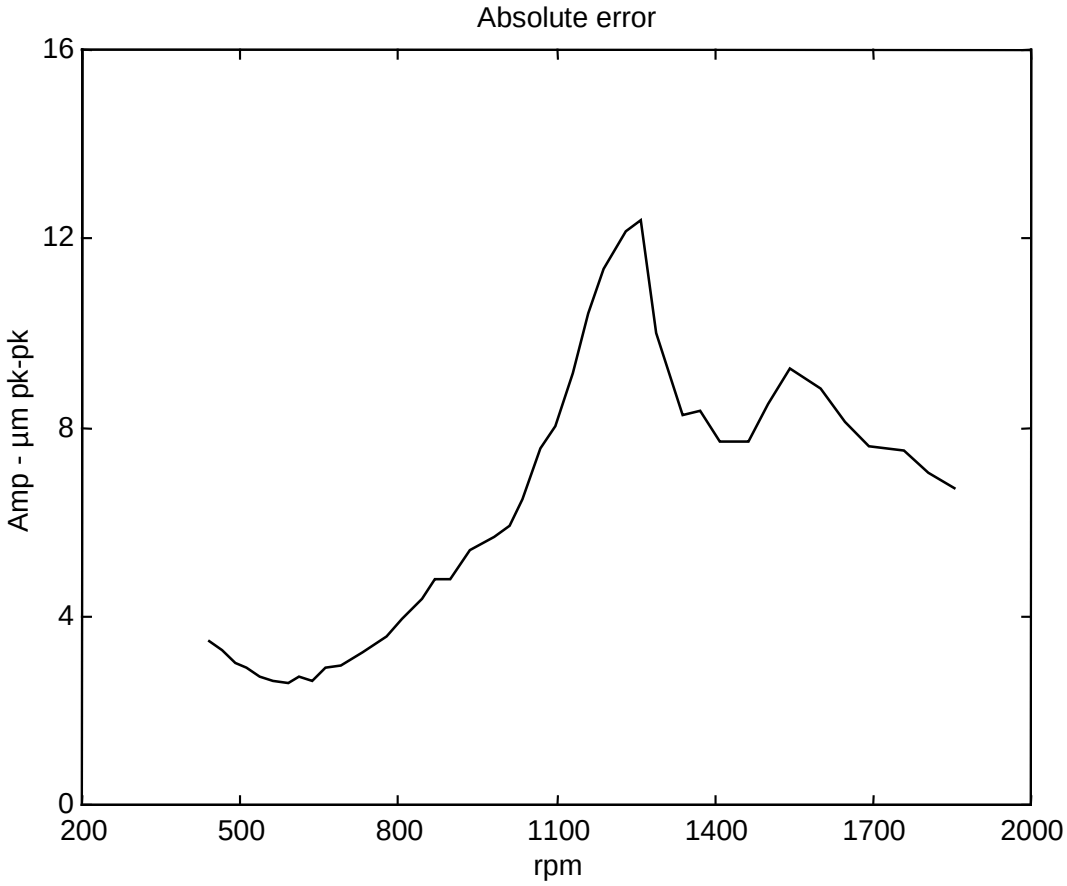

Figure 16. Absolute error vs. rotating speed.

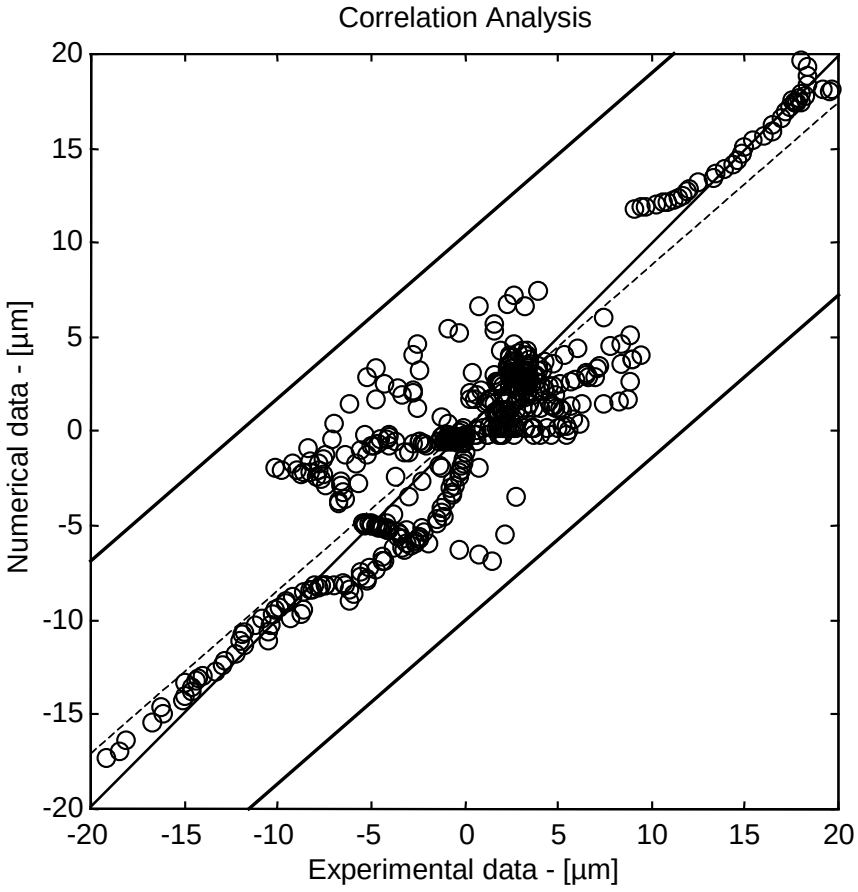

Figure 17. Correlation analysis between numerical and experimental vibration data.

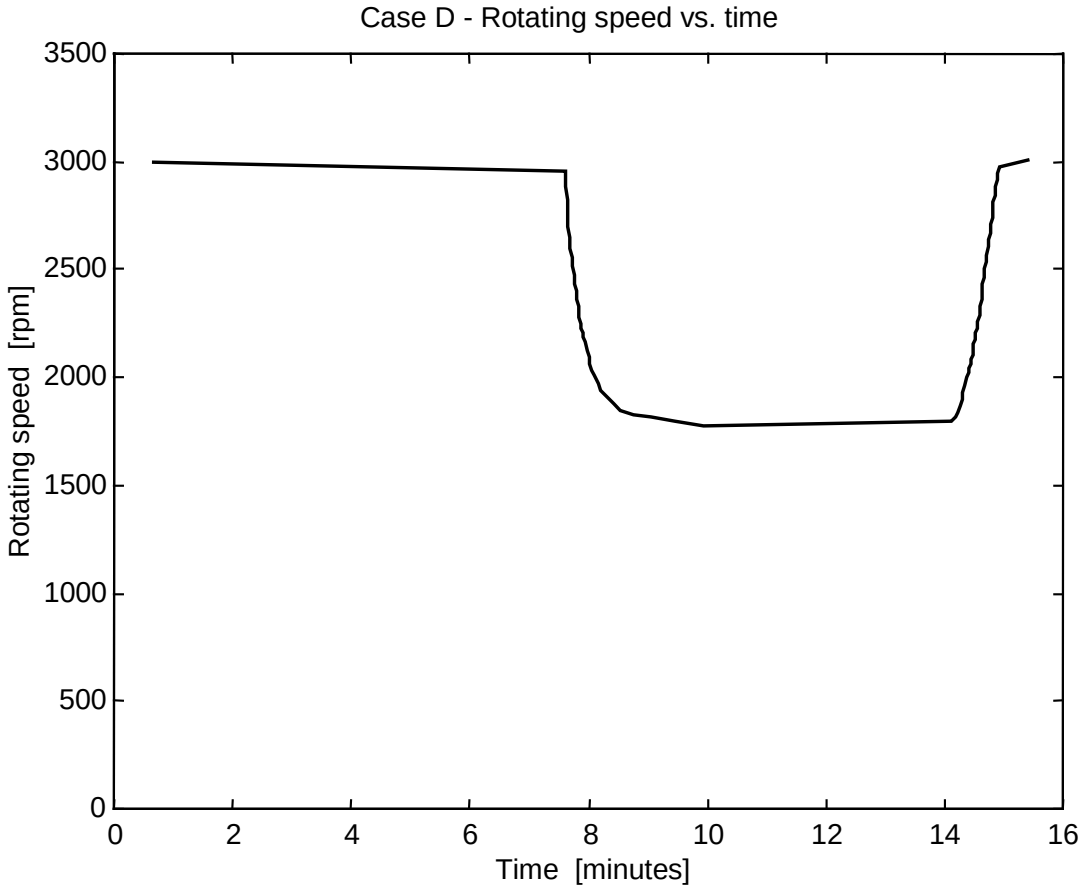

Figure 18. Generator rotating speed vs. time, during the partial coastdown and the subsequent runup.

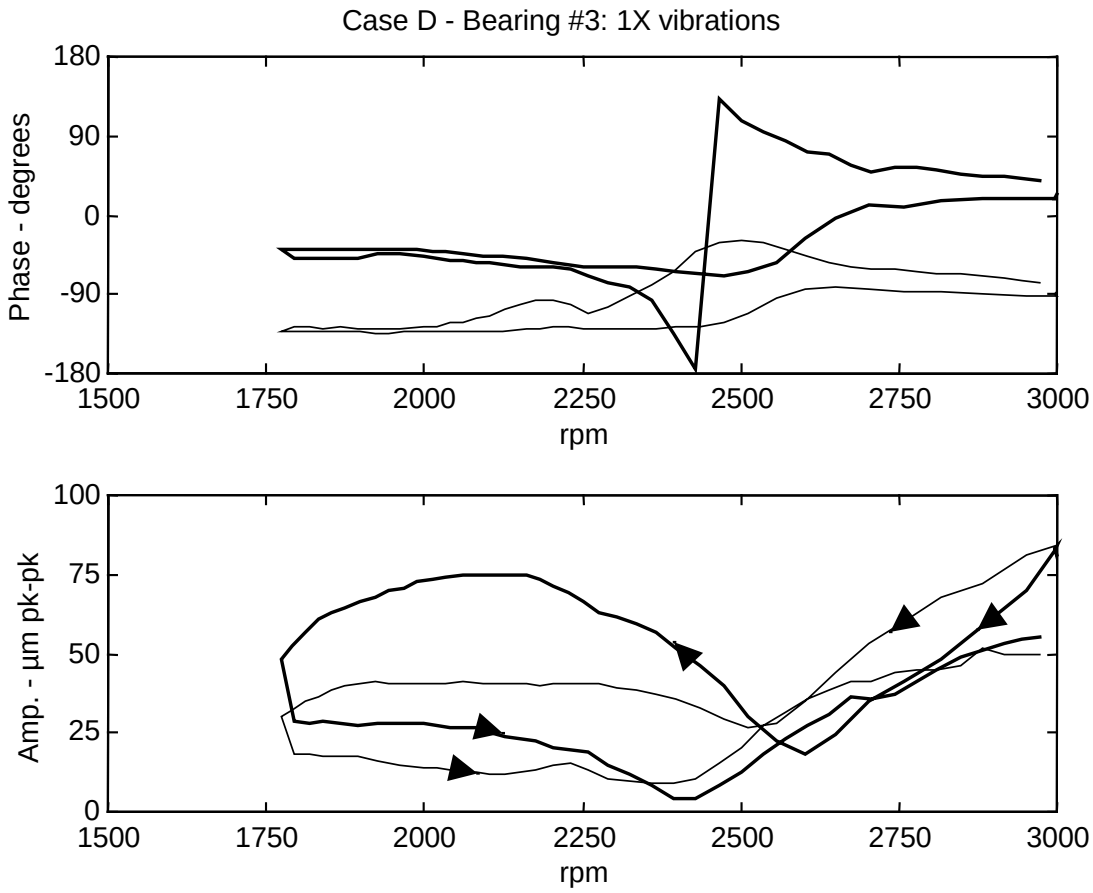

Figure 19. Bode plot of the 1X vibrations measured at bearing #3, in X and Y direction, during the partial coastdown and the subsequent runup (Case D). Thick line: X direction (45°R). Fine line: Y direction (45°L).

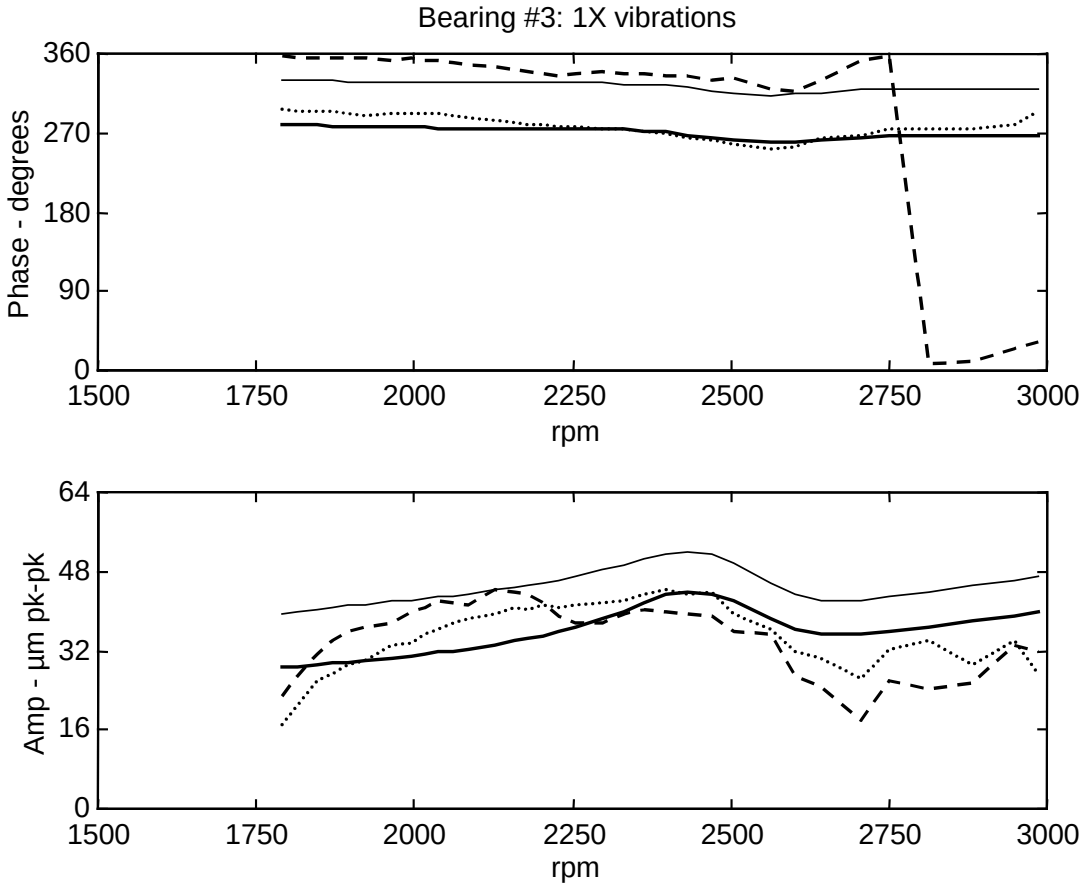

Figure 20. Additional vibrations (1X) at bearing #3. Comparison between experimental vibrations and numerical results obtained with the identified fault. Dotted line: horizontal experimental vibrations. Dashed line: vertical experimental vibrations. Thick line: horizontal theoretical vibrations. Fine line: vertical theoretical vibrations.